Published 03/28/2017

doi:10.4271/2017-01-0578
saefuel.saejournals.org

Numerical Investigation of a Gasoline-Like Fuel in a Heavy-Duty Compression Ignition Engine Using Global Sensitivity Analysis

Pinaki Pal
Argonne National Laboratory

Daniel Probst
Convergent Science Inc.

Yuanjiang Pei
Aramco Research Center

Yu Zhang
Aramco Services Co.

Michael Traver
Aramco Research Center

David Cleary
Aramco Services Co.

Sibendu Som
Argonne National Laboratory

ABSTRACT

Fuels in the gasoline auto-ignition range (Research Octane Number (RON) > 60) have been demonstrated to be effective alternatives to diesel fuel in compression ignition engines. Such fuels allow more time for mixing with oxygen before combustion starts, owing to longer ignition delay. Moreover, by controlling fuel injection timing, it can be ensured that the in-cylinder mixture is “premixed enough” before combustion occurs to prevent soot formation while remaining “sufficiently inhomogeneous” in order to avoid excessive heat release rates. Gasoline compression ignition (GCI) has the potential to offer diesel-like efficiency at a lower cost and can be achieved with fuels such as low-octane straight run gasoline which require significantly less processing in the refinery compared to today’s fuels.

To aid the design and optimization of a compression ignition (CI) combustion system using such fuels, a global sensitivity analysis (GSA) was conducted to understand the relative influence of various design parameters on efficiency, emissions and heat release rate. The design parameters included injection strategies, exhaust gas recirculation (EGR) fraction, temperature and pressure at intake valve closure and injector configuration. These were varied simultaneously to achieve various targets of ignition timing, combustion phasing, overall burn duration, emissions, fuel consumption, peak cylinder pressure and maximum pressure rise rate. The baseline case was a three-dimensional closed-cycle computational fluid dynamics (CFD) simulation with a sector mesh at medium load conditions. Eleven design parameters were considered and ranges of variation were prescribed to each of these. These input variables were perturbed in their respective ranges using the Monte Carlo (MC) method to generate a set of 256 CFD simulations and the targets were calculated from the simulation results. GSA was then applied as a screening tool to identify the input parameters having the most significant impact on each target. The results were further assessed by investigating the impact of individual parameter variations on the targets. Overall, it was demonstrated that GSA can be an effective tool in understanding parameters sensitive to a low temperature combustion concept with novel fuels.

CITATION: Pal, P., Probst, D., Pei, Y., Zhang, Y. et al., "Numerical Investigation of a Gasoline-Like Fuel in a Heavy-Duty Compression Ignition Engine Using Global Sensitivity Analysis," *SAE Int. J. Fuels Lubr.* 10(1):2017, doi:10.4271/2017-01-0578.

INTRODUCTION

The transportation industry accounts for around 20% of the total energy consumed globally [1]. It is expected that the global demand for transport energy will rise by ~40% by 2040. Moreover, in the foreseeable future, internal combustion (IC) engines using liquid fuels made from petroleum are expected to dominate the transport sector [2, 3, 4, 5, 6]. Given the focus on reducing greenhouse gas (GHG) emissions in the transportation industry, there is a need for more efficient IC engines for both passenger and commercial applications. This pursuit of higher efficiency has led to a stronger interest in advanced compression-ignition (CI) engines. CI engines are more fuel-efficient than the spark-ignited (SI) engines due to their relatively high compression ratios and lack of throttling losses. However, conventional CI engines suffer from higher emissions of nitrogen oxides (NO_x) and particulate matter (PM) due to local fuel-rich combustion and higher in-cylinder temperatures. Modern diesel engines use exhaust gas recirculation (EGR) to lower the in-cylinder temperature and oxygen content so that NO_x is reduced. However, this adversely affects the oxidation of any soot that is formed in the cylinder.

To address the combined needs of further emissions reduction, improved efficiency and cost, alternative forms of CI combustion are being explored [7, 8]. Gasoline compression ignition (GCI) [9] is one of the most attractive alternative combustion strategies, and can use fuels in the gasoline auto-ignition range (RON > 60) instead of a diesel fuel in a CI engine. The longer ignition delay of such fuels allows more time for mixing before combustion starts [10, 11, 12]. In addition, sufficient inhomogeneity in the fuel-air mixture can be ensured by late fuel injection so that combustion will occur somewhere in the cylinder and will promote combustion of the rest of the charge. At the same time, the in-cylinder mixture is "homogeneous enough" everywhere in the cylinder before combustion starts so that soot formation is circumvented [8]. Therefore, GCI has the potential to offer diesel-like efficiency at lower cost by using low-octane, low-cetane, gasoline-like fuels that may require less processing in the refinery compared to today's fuels. Utilization of such fuels could lead to significant energy savings in fuel manufacturing. In addition, the fuel injection pressures need not be as high as with diesel fuel [13, 14, 15] as longer fuel ignition delay already facilitates better mixing. This can reduce the cost of the fuel injection system for GCI.

However, GCI combustion is dependent on a number of engine design parameters such as fuel injection strategies, EGR levels, intake temperature and pressure, and injector configuration. Different combinations of these parameters can lead to a variety of combustion characteristics, emissions and pressure rise rates. Engine simulation is a valuable tool that can aid the development of advanced combustion strategies such as GCI. Computational fluid dynamics (CFD) is being commonly used in the industry, thereby serving to shorten product development cycle and delivering significant cost savings as compared to experimental prototyping.

The influence of a large number of input parameters on specific targets of interest can be assessed using sensitivity analysis. Sensitivity analysis has been used in the chemical kinetics community as a technique for uncertainty quantification [16, 17, 18]. The goal in these studies was to identify reactions in large chemical kinetic mechanisms which influenced the ignition delay timing the most, so that the rate constants for those reactions could be computed with greater fidelity. This, in turn, led to the development of improved and more predictive chemical kinetic mechanisms.

In the past, diesel engine simulations have employed the local sensitivity analysis method to study the effect of a few parameters sequentially such as spray breakup and combustion model constants [19] to provide a guideline on how to calibrate the models under these conditions. However, this approach inherently cannot incorporate any non-linear effects. In this regard, global sensitivity analysis (GSA) has significant advantages over the traditional local sensitivity analysis approaches such as brute force methods [20]. It provides a more realistic picture by accounting for the uncertainties in all the relevant parameters considered simultaneously. Moreover, it captures the non-linear response of targets to the input parameters. Pei el al. [21] applied global sensitivity analysis to an engine simulation for the first time to quantify the sensitivities of various target functions such as ignition delay, combustion phasing and emissions to various inputs such as experimental boundary conditions, fuel properties and CFD model constants. Later, Pei et al. [22] carried out a similar study using GSA to quantify the uncertainties for the Engine Combustion Network (ECN) Spray A [23]. More recently, Kodavasal et al. [24, 25] explored the effect of uncertainties in experimental boundary conditions and fuel properties on GCI operation with conventional gasoline fuel using a similar approach for a light-duty engine. These studies demonstrated that GSA could be employed as a valuable tool to readily identify important parameters which have the greatest influence on engine combustion behavior. However, the engine combustion sensitivity to various design parameters when utilizing a low-octane gasoline-like fuel is expected to be different and hasn't been explored previously.

Therefore, in the present work, GSA was applied to CFD simulation of a heavy-duty CI engine at medium load conditions operating with a low-octane gasoline-like fuel. A number of key design parameters are considered and their relative influences on specific targets of efficiency, emissions and heat release rate are quantified. The main objective is to provide direction on which control variables have the highest impact on the combustion characteristics, thereby requiring the highest attention during engine design and optimization phase. The paper is arranged as follows. Firstly, the engine setup is briefly discussed and details of the numerical model are provided. This is followed by a brief overview of the GSA methodology employed in this work. Next, the input parameters and their respective ranges of variation are prescribed. Then, the CFD model setup is validated against experimental data. Subsequently, the results of the GSA are discussed in terms of the sensitivity of target variables to the input parameters. Brute force sensitivity analysis is also performed on some important variables to gain additional insights. The paper concludes with a summary of the main findings.

METHODOLOGY

Engine Setup

The experimental data were generated using a four-stroke, six-cylinder, heavy-duty Cummins test engine with a variable-geometry turbocharger, high-pressure cooled EGR loop and charge air cooler. A nine-hole mini-sac injector nozzle was used. The details of the engine geometry and operating conditions for the baseline case on which the GSA was performed are listed in Table 1. The in-cylinder pressure and emissions data were used to validate the CFD model described in the next section.

Table 1. Engine specifications and operating conditions.

Engine model	Cummins ISX15
Cylinders	6
Displacement	14.9 l
Bore	137 mm
Stroke	169 mm
Connecting Rod	262 mm
Compression ratio	17.3:1
Engine speed	1375 rpm
Intake valve closing	-137 ^{0}CA aTDC
Exhaust valve opening	148 ^{0}CA aTDC
Start of injection timing	-9 ^{0}CA aTDC
Injection duration	15.58 ^{0}CA
Mass of fuel injected	0.1245 g/cycle/cylinder
Fuel injection temperature	360 K
Injection pressure	1600 bar
Nozzle inclusion angle	152^0
IVC pressure	323 K
IVC temperature	2.15 bar
EGR	41%
Global equivalence ratio	0.57

Numerical Model Setup

A commercial 3-D CFD code, CONVERGE (version 2.3.8) [26], is used to perform numerical simulations for the closed part of the cycle, from intake valve closing (IVC) to exhaust valve opening (EVO). Assuming axisymmetry, the simulation domain is considered to be a sector mesh representing a single cylinder and accounting for only one spray plume in order to reduce the computational expense. Periodic boundary conditions are imposed in the azimuthal direction. A uniform mixture and temperature distribution is specified at IVC.

CONVERGE uses a modified, cut-cell Cartesian method for grid generation directly during runtime. In addition, it has the capability to include fixed embedding of cells, i.e., increasing the grid resolution with respect to base grid size *a priori* along the cylinder walls and near the nozzle, and adaptive mesh refinement (AMR) to refine areas where the sub-grid field is largest [26]. In the present work, a base mesh size of 1.4 mm is used. One level of fixed embedding is prescribed near the cylinder head and piston, while two levels of fixed embedding are employed to resolve the flow near the fuel injector. In addition, two levels of AMR are employed based on the velocity and temperature sub-grid scales of 1 m/s and 2.5 K, respectively. This results in the minimum grid size of 0.35 mm. The computational mesh for the baseline case at top-dead-center (TDC) is shown in Figure 1. The simulation time step is automatically adjusted in the simulations based on the maximum convective, diffusive and mach Courant-Friedrichs-Lewy (CFL) numbers of 1, 2 and 50, respectively.

In-cylinder turbulence is modeled using the Reynolds-Averaged Navier Stokes (RANS) based re-normalized group (RNG) k-ε model [27] with wall functions. The liquid spray is treated in a Lagrangian fashion and the "blob" injection model by Reitz and Diwakar [28] is used, which initializes the diameter of a liquid droplet to the effective nozzle diameter. The Kelvin Helmholtz (KH) – Rayleigh Taylor (RT) breakup model [29, 30] and "no-time counter" collision model of Schmidt and Rutland [31] are employed to describe the subsequent spray atomization and collision processes, respectively. Droplet evaporation is modeled using Frossling correlation [32] and models are also included for dynamic drop drag [33] and droplet turbulent dispersion [34]. A reduced chemical kinetic mechanism for primary reference fuel (PRF) consisting of 48 species and 152 reactions based on Liu et al. [35] is used in this work. A RON70 two-component surrogate comprising of 70% iso-octane by mass and 30% n-heptane by mass is employed [36]. In addition, the NO_x formation is modeled by the extended Zel'dovich mechanism [37]. The empirical Hiroyasu soot model [38] coupled with the Nagle and Strickland-constable model [39] are used to determine the soot formation and oxidation rates and acetylene (C2H2) is considered as the precursor for soot formation. For combustion modeling, the SAGE detailed chemistry solver [40] is employed along with a multi-zone (MZ) approach, with bins of 5 K in temperature and 0.05 in equivalence ratio [26, 41]. Although it doesn't utilize an explicit turbulent combustion closure [42, 43, 44], the SAGE-MZ model has been demonstrated to perform well to simulate spray combustion in the context of RANS in some previous studies [45].

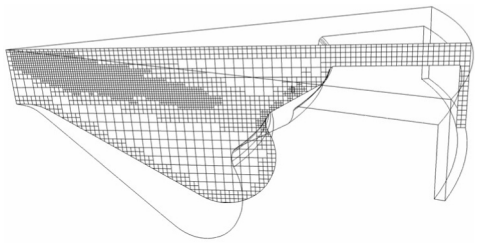

Figure 1. Computational mesh for the baseline case at TDC.

GSA Methodology

GSA is used as a tool to explore the relations between the input parameters and the outputs/targets of a model. This approach is more insightful than the local sensitivity analysis methods [46], where only a single input parameter is varied, as it captures the relative sensitivity of different variables on the targets of interest over the whole input parameter space. In doing so, it also accounts for the non-linear response of targets to the input variables. The details of the GSA methodology can be found in Ref. [16]. However, a brief discussion is provided as follows.

Assume that there are 'n' input parameters and each one of them is equally likely to lie anywhere within a prescribed range of variation:

$$\upsilon_i \in \left[\upsilon_i^L \upsilon_i^H\right], i = 1, 2, ..., n, \tag{1}$$

where υ_i is the ith variable, v_i^L and v_i^H are the lower and higher limits of its range of variation, respectively. It is assumed that the probability distribution of the parameters is uniform within the n-dimensional hypercube [16]:

$$\Omega \in \left[\upsilon_1^L \upsilon_1^H\right] \otimes ... \otimes \left[\upsilon_i^L \upsilon_i^H\right] \otimes ... \otimes \left[\upsilon_n^L \upsilon_n^H\right] \tag{2}$$

The Monte Carlo method is used to generate a large number 'N' of independent random parameter sets within the above hypercube for CFD simulations. In the present study, 256 simulations are used, i.e., $N = 256$. The targets obtained from the simulations can be written as:

$$f = f(\upsilon), \tag{3}$$

where f is the vector of targets of interest and υ is the vector containing one set of the sampled n input parameters. The GSA is implemented based on the analysis of variance using an ordinary least squares (OLS) method through the following expansion:

$$f(\upsilon_i) = \sum_{i=1}^{n} \sum_{k=0}^{m} a_{ik} \upsilon_i^k, \tag{4}$$

where m is the order of expansion. Here, $m = 2$. The sensitivity coefficient of each input parameter (S_i) can then be computed as the ratio of the partial variance to the total variance as shown below:

$$S_i = \sigma_i^2 / \sigma_t^2, \tag{5}$$

$$\sigma_t^2 = \left\langle f^2 \right\rangle - \left\langle f \right\rangle^2, \tag{6}$$

where the brackets "< >" indicate the mean value over N simulations. In Eq. (5), σ_i^2 denotes the partial variance of i^{th} parameter based on the expansion shown in Eq. (4). The larger the sensitivity coefficient, the greater the impact an input variable has on a particular target function. It must be noted that the range of variation imposed on the inputs can influence the relative values of the sensitivity coefficients.

Control Variables and Their Ranges

The design parameters used as control variables in the present study along with their respective ranges of variation are listed in Table 2. In total, eleven input variables are chosen pertaining to fuel injector design (number of nozzle holes, total nozzle area, nozzle inclusion angle), fuel injection strategy (injection pressure, start-of-injection (SOI) timing) and initial conditions (IVC temperature and pressure, EGR fraction, initial turbulence level and swirl). Each parameter is assigned a minimum and maximum value. The ranges of variation include the baseline conditions. The total nozzle area and initial turbulence kinetic energy (TKE, k) are normalized with respect to the respective baseline values, therefore the baseline values are 1. Figure 2 shows the distributions generated for P_{IVC} and EGR. It is evident that these variables are randomly distributed using the MC method over the sample space identified by their ranges of variation. The other input parameters also have similar random distributions.

Table 2. Control variables and respective ranges of variation along with the baseline setup.

Variable	Description	Baseline	Min.	Max.
N_{holes}	Number of nozzle holes	9	8	10
A_{noz}	Total nozzle area	1	1	1.3
P_{inj}	Injection pressure [bar]	1600	1400	1800
SOI	Start-of-injection timing [^{0}CA aTDC]	-9	-13	-5
θ_{noz}	Nozzle inclusion angle [^{0}]	152	148	156
EGR	EGR fraction	0.41	0.35	0.50
T_{IVC}	IVC temperature [K]	323	323	373
P_{IVC}	IVC pressure [bar]	2.15	2.0	2.3
TKE, k	Initial turbulent kinetic energy	1	0.7	1.3
L_{turb}	Initial turbulence length scale [mm]	4.5	1	8
SR	Swirl ratio	1	1	2.4

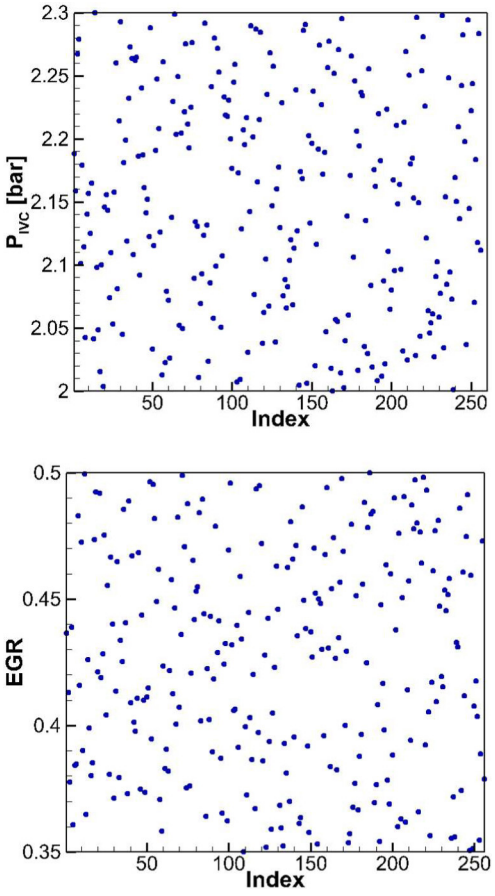

Figure 2. MC distributions of IVC pressure (top) and EGR fraction (bottom) for the 256 simulation cases.

Automated Simulation Case Setup

The initial turbulence length scale (L_{turb}) is used in the calculation of turbulent dissipation rate (ε in the k-ε turbulence model). The dissipation rate is inversely proportional to L_{turb}. The composition at

IVC is computed based on the EGR fraction, T_{IVC}, P_{IVC} and total mass of fuel injected. Also, it must be noted that in the CONVERGE CFD code, nozzle diameter, duration of injection (DOI) and injection velocity rate-shape are the inputs that need to be prescribed. These CFD model inputs are computed from the first three input parameters listed in Table 2 as follows. For a particular simulation case, first the nozzle diameter is calculated based on the total nozzle area and number of nozzle holes. The number of nozzle holes also determines the sector mesh to be used for that particular case, which is generated using CONVERGE's Make Surface utility [26]. In addition, this also provides the fuel mass injected in the sector domain because the total mass injected is constant and each nozzle hole injects the same mass of the fuel. Now, due to the A_{noz} and P_{inj} scaling, the fuel mass flow rate-shape changes from the baseline case. Hence, in order to meet the updated mass injected per nozzle hole, the baseline mass flow rate-shape is modified by iteratively removing (or adding) data points from (or to) the "quasi-steady" portion of the rate-shape, thereby causing the DOI to change accordingly. Finally, the DOI is again adjusted slightly to match the injection pressure. Figure 3 shows the resultant injection velocity and injection pressure profiles for two extreme scenarios over the input parameter space (Scenario A: N_{holes} = 8, A_{noz} = 1.3, P_{inj} = 1800 bar) and (Scenario B: N_{holes} = 10, A_{noz} = 1, P_{inj} = 1400 bar), along with the corresponding baseline profiles.

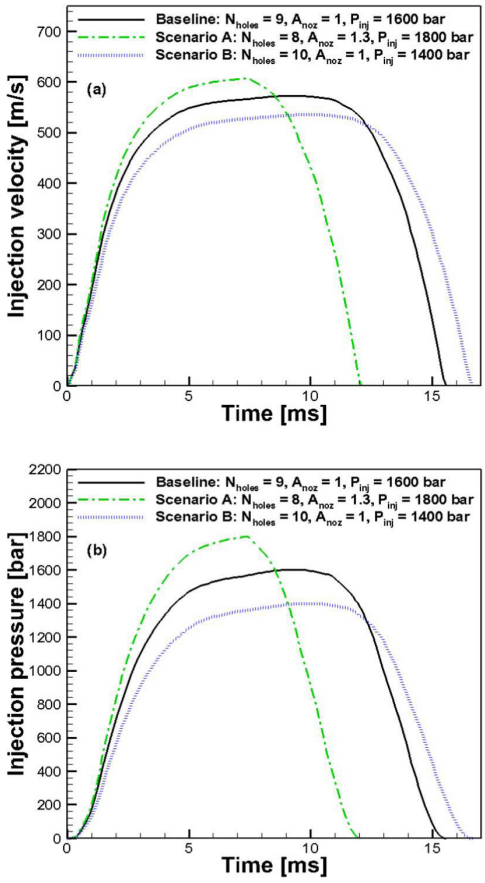

Figure 3. (a) Fuel injection velocity and (b) fuel injection pressure profiles generated by CONVERGE CONGO setup. Corresponding baseline profiles are also shown for reference.

A standalone code is developed using the CONVERGE genetic optimization utility, CONGO [26], to perform all the operations described above in this section for each of the 256 simulation cases sequentially and generate the respective input files. All the simulations were run concurrently on half of a rack of Mira, an IBM BG/Q supercomputer at Argonne Leadership Computing Facility (ALCF) and Office of Science User Facility at Argonne, with each case running on 32 cores (2 nodes, 16 cores per node). The average runtime per simulation was around 72 hours. In order to ensure that the sample size provided convergent results, the GSA was performed on a smaller subset (128 simulations) as well. It was found that the relative sensitivities of various targets to the inputs did not change between the two sets. This confirmed that 256 simulations provided a *big enough* sample set for the present study. Moreover, 20 simulation cases based on the maximum, minimum and baseline values of each input variable from Table 2 were also run for brute force sensitivity analysis to further quantify the influence of independent variations in input parameters on the targets. We note that independent variations are not practical but they do provide us with further insights.

RESULTS AND DISCUSSION

Model Validation

The CFD model predictions were validated against experimental data for RON70 naphtha at the baseline conditions. As seen in Figure 4, cylinder pressure traces and heat release rates predicted by the CFD model were in good agreement with the experimental results. In addition, Figure 5 showed that the model was also able to capture the engine-out NO_x and soot emissions reasonably well.

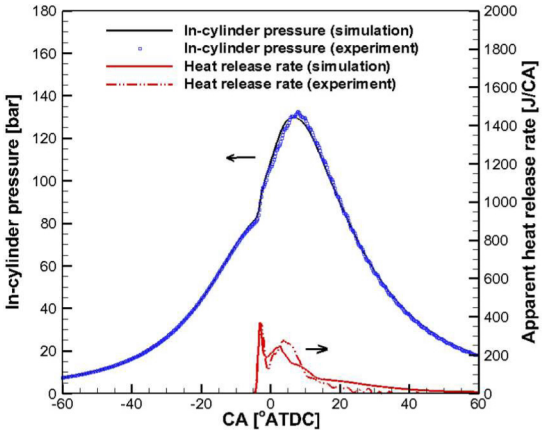

Figure 4. Comparison of numerical and experimental in-cylinder pressure traces for RON70 naphtha at baseline conditions.

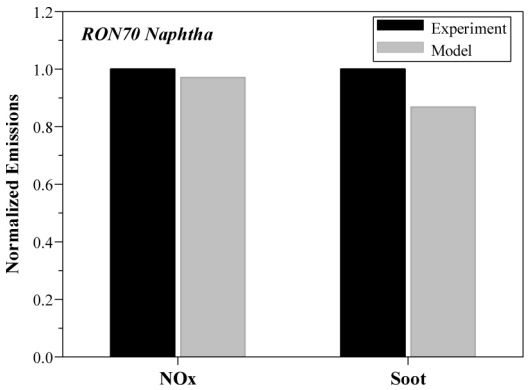

Figure 5. Comparison of NO_x and soot emissions for RON70 naphtha at baseline conditions.

GSA Results

A number of targets such as ignition timing, combustion phasing, burn duration, emissions, fuel consumption, peak cylinder pressure and maximum pressure rise rate are discussed and their responses to the input parameters are analyzed. The results are presented in terms of bar plots showing the sensitivity of targets to different inputs and scatter plots with regression fits of the targets versus the input variables they are most sensitive to.

Ignition Timing

CA2 and CA10 can be used as the two definitions for ignition timing. They correspond to the crank angles when 2% and 10% of the total integrated heat release occur, respectively. CA10 is typically easier to measure from experiments and is a more conventional definition of ignition timing. However, CA2 is indicative of the first stage of heat release, which is interesting from a chemical kinetics viewpoint.

The sensitivity coefficients for the input variables affecting CA2 and CA10 are reported in Figure 6. Clearly, both quantities are predominantly sensitive to SOI timing. Other input variables play negligible roles in influencing ignition timing with sensitivity coefficients less than 0.1. Figure 7 shows the scatter plots of CA2 and CA10 versus SOI and the corresponding regression fits. As the SOI is delayed, ignition timing expectedly gets retarded. Also, the spread in CA10 is higher than that in CA2. The spread is influenced by other input variables and higher spread means a larger effect of others at a certain SOI timing. Higher spread for CA10 is expected due to greater combustion progress in the cylinder. Unlike CA2, CA10 also shows some degree of controllability through EGR, T_{IVC} and P_{IVC}, as shown in Figure 6.

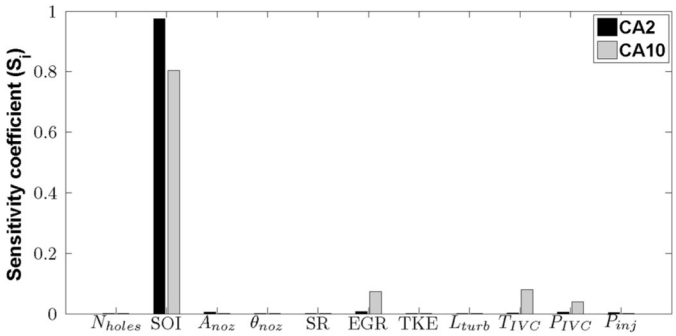

Figure 6. Sensitivity coefficients of different input variables for ignition timing.

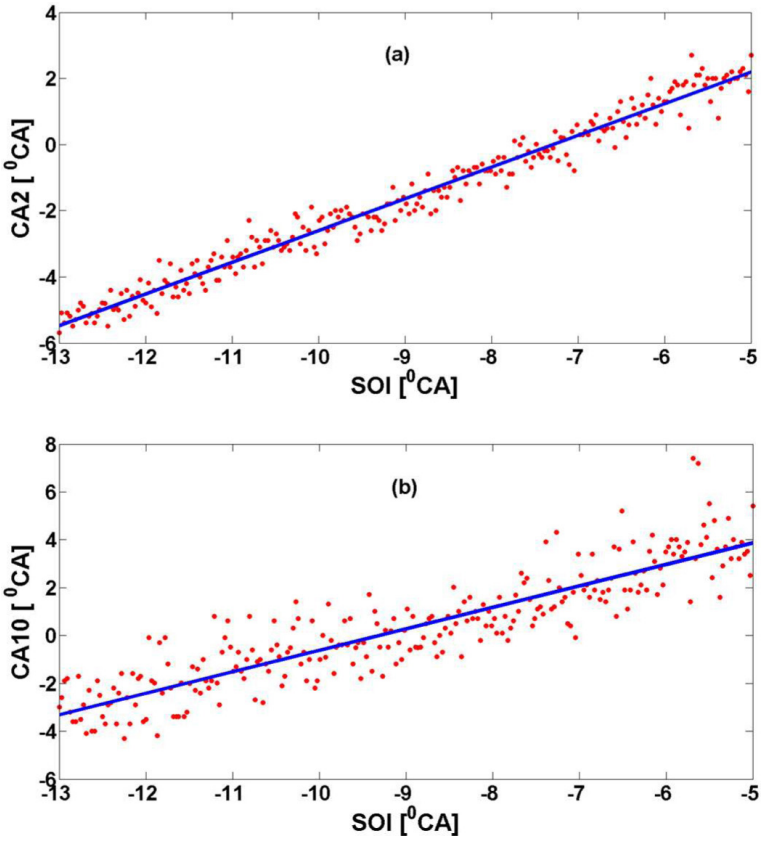

Figure 7. Scatter plots of [a] CA2 and [b] CA10 versus SOI. The blue curves are the corresponding regression fits.

Combustion Phasing and Burn Duration

The next set of targets are for combustion phasing, CA50 and CA90, which are key indicators of the progress in combustion. These correspond to the crank angles for 50% and 90% of total heat release, respectively.

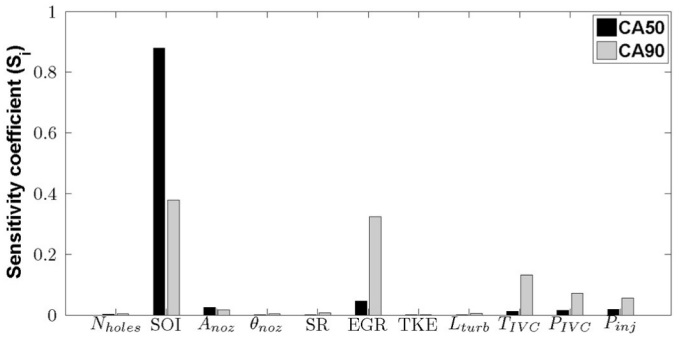

Figure 8. Sensitivity coefficients of different input variables for combustion phasing.

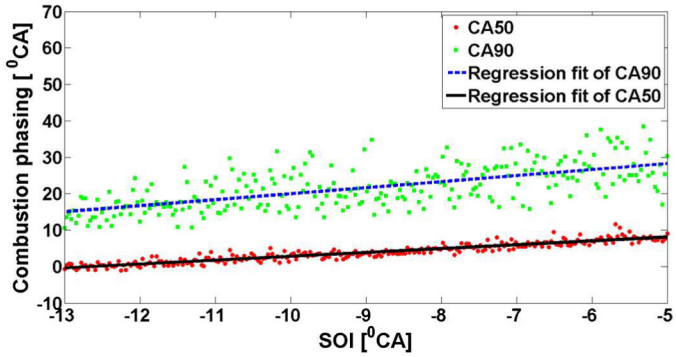

Figure 9. Scatter plots of CA50 and CA90 versus SOI. The blue and black curves are the corresponding regression fits.

Figure 8 shows the sensitivity of these two target quantities towards the control variables. CA50 is found to be strongly correlated to SOI, which is also suggested by the very narrow spread in Figure 9. Increasing SOI linearly increases the CA50 as depicted in Figure 9. This is consistent with the effect of SOI on CA2 and CA10 as observed earlier. Figures 8 and 9 indicate that CA90 is most sensitive to SOI as well, with a trend similar to CA50. The spread is higher for CA90 compared to CA50 though, which is consistent with the findings corresponding to Figure 7. CA90 is also significantly influenced by EGR and T_{IVC}. In particular, the sensitivities of CA90 to SOI and EGR are nearly equal. It can be seen in Figure 10 that CA90 gets delayed with both increasing EGR fraction and higher T_{IVC}. An increase in either of these input parameters would lead to higher residual (CO_2 and H_2O) mass fraction in the cylinder at IVC. This would tend to lower the in-cylinder temperatures and cause slower rate of overall heat release. It is also noted from Figure 8 that CA90 is more sensitive to EGR as compared to T_{IVC}. This is probably due to the fact that with an increase in T_{IVC}, the in-cylinder mixture would be at a higher temperature at IVC. Hence, the net cooling effect is expected to be less pronounced as compared to a scenario where EGR fraction is raised while keeping T_{IVC} constant.

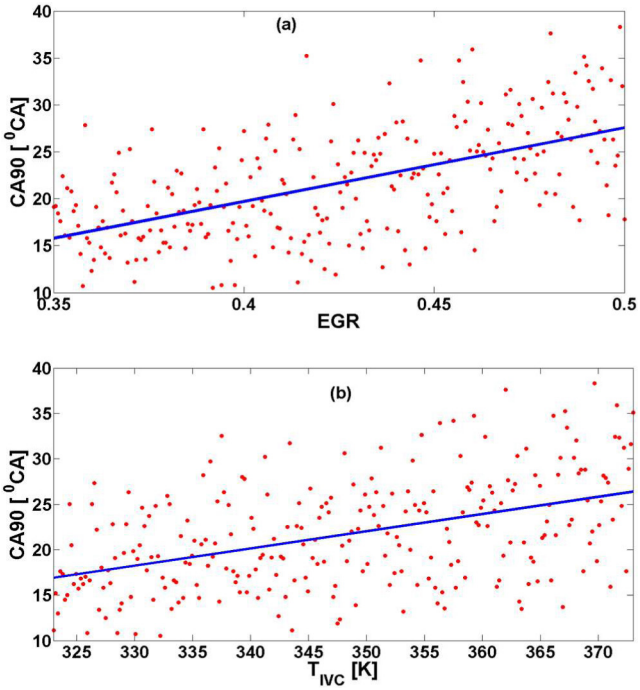

Figure 10. Scatter plots of CA90 versus [a] EGR and [b] T_{IVC}. The blue curves are the corresponding regression fits.

In addition to combustion phasing, the impact of input parameters on overall combustion burn duration is also assessed, as shown in Figure 11. Here, CA 2-90 is used as a metric for burn duration. Clearly, it is most sensitive to EGR and T_{IVC}. Higher EGR and T_{IVC} result in more prolonged burn duration as shown in Figure 12. These trends are similar to those observed for CA90 and can be justified based on similar reasoning as above. Burn duration also shows a moderate level of sensitivity to P_{IVC} and P_{inj}.

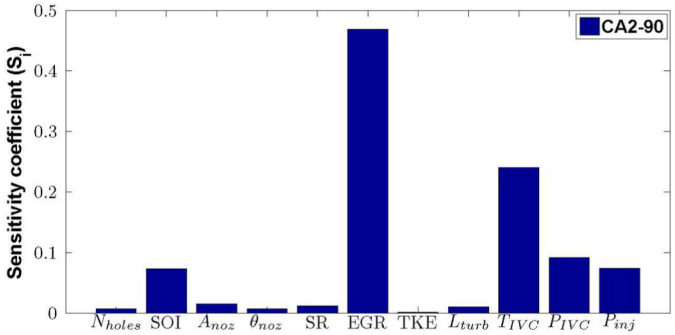

Figure 11. Sensitivity coefficients of different input variables for CA2-90 combustion burn duration.

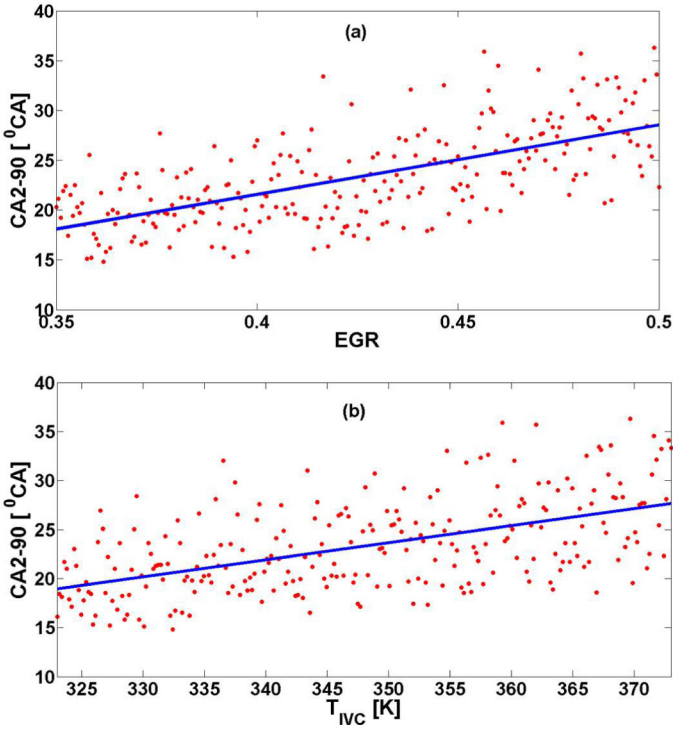

Figure 12. Scatter plots of CA2-90 versus [a] EGR and [b] T_{IVC}. The blue curves are the corresponding regression fits.

Emissions and Fuel Consumption

First, NO_x and soot emissions are examined. The sensitivity coefficient results in Figure 13 clearly indicate that NO_x emissions are primarily sensitive to EGR fraction, whereas both T_{IVC} and EGR have a pronounced effect on soot emissions. A scatter plot of NO_x with respect to EGR is shown in Figure 14. NO_x emissions tend to be lowered by a higher percentage of EGR, which has also been observed for conventional diesel combustion. This is primarily attributed to the lowering of burned gas temperatures due to higher residual fraction. On the other hand, as depicted in Figure 15 (a), soot emissions increase with increase in EGR, which is mainly the result of suppressed soot oxidation due to lower combustion temperatures and lower oxygen concentration.

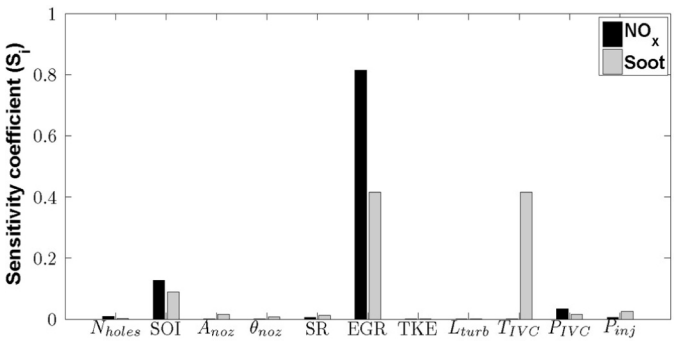

Figure 13. Sensitivity coefficients of different input variables for NO_x and soot emissions.

Soot emissions are also influenced by T_{IVC} in that higher T_{IVC} leads to more soot as shown in Figure 15 (b). This can be explained by Figure 16 which shows the in-cylinder distributions of equivalence ratio and soot mass fraction at 15 °CA aTDC, from brute force sensitivity analysis performed for the minimum and maximum T_{IVC} in the prescribed range of variation as noted in Table 2. It is observed that higher T_{IVC} results in lower oxygen content in the in-cylinder mixture and thereby more fuel-rich regions ($\Phi > 1$) during the combustion phase. This promotes higher soot formation. This fact is further demonstrated in Figure 17, which shows the temporal evolution of in-cylinder soot for the bounded values of T_{IVC}.

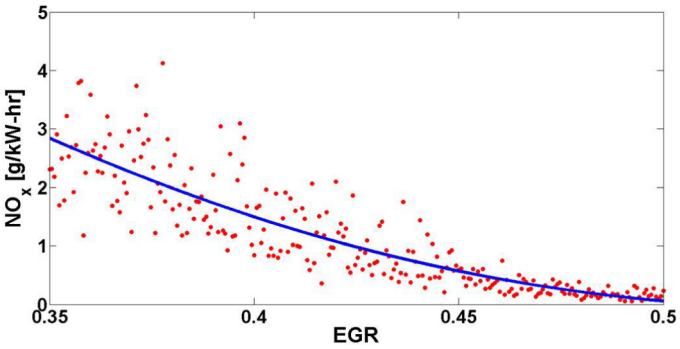

Figure 14. Scatter plot of NO_x emissions versus EGR. The blue curve is the corresponding regression fit.

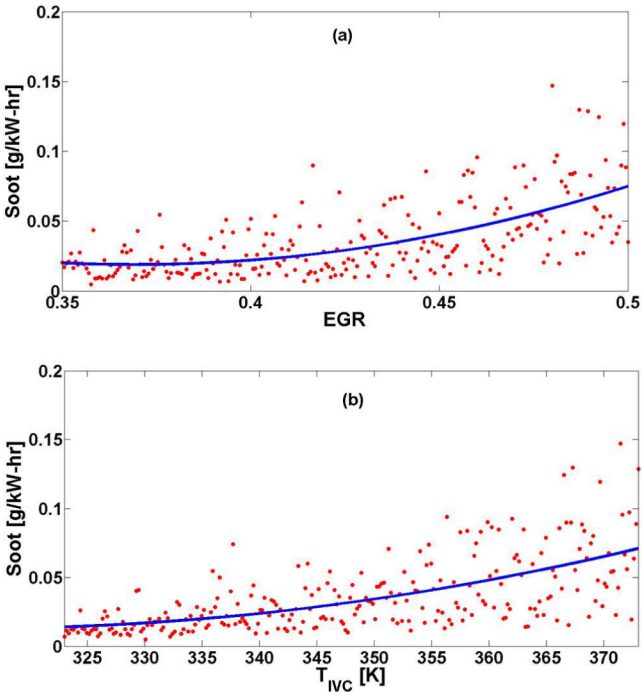

Figure 15. Scatter plots of soot emissions versus [a] EGR and [b] T_{IVC}. The blue curves are the corresponding regression fits.

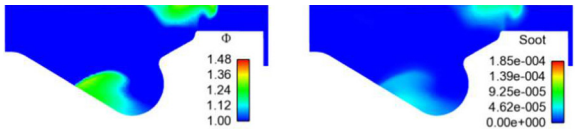

a.

Figure 16. In-cylinder equivalence ratio and soot mass fraction distributions along a cut-plane at 15 °CA aTDC for the [a] minimum (323 K) and [b] maximum (373 K) values of T_{IVC} noted in Table 2. All other input parameters are same as in the baseline case.

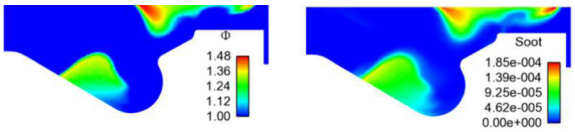

b.

Figure 16. (cont.) In-cylinder equivalence ratio and soot mass fraction distributions along a cut-plane at 15 °CA aTDC for the [a] minimum (323 K) and [b] maximum (373 K) values of T_{IVC} noted in Table 2. All other input parameters are same as in the baseline case.

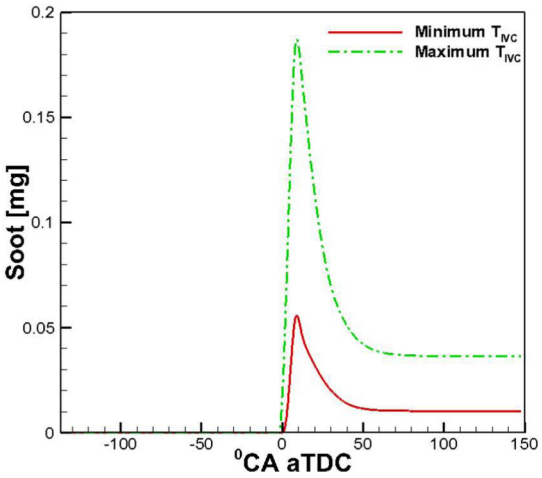

Figure 17. Temporal evolution of soot for the minimum (323 K) and maximum (373 K) values of T_{IVC} noted in Table 2.

Next, the impact of input parameters on carbon monoxide (CO) and unburned hydrocarbon (UHC) emissions is explored. The sensitivity coefficient results in Figure 18 show that CO emissions are mostly influenced by EGR with some minor sensitivity to swirl ratio and nozzle inclusion angle. Higher amount of residuals in the in-cylinder mixture favors CO formation as indicated by Figure 19. Higher EGR causes lower oxygen concentration resulting in more fuel-rich combustion and thereby an increased CO production. At the same time, it causes lower bulk gas temperatures leading to incomplete CO-CO2 conversion. It is noted that the regression fit in Figure 19 shows a non-linear effect.

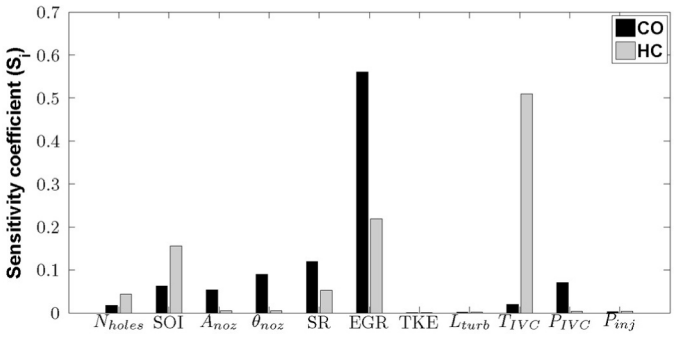

Figure 18. Sensitivity coefficients of different input variables for CO and HC emissions.

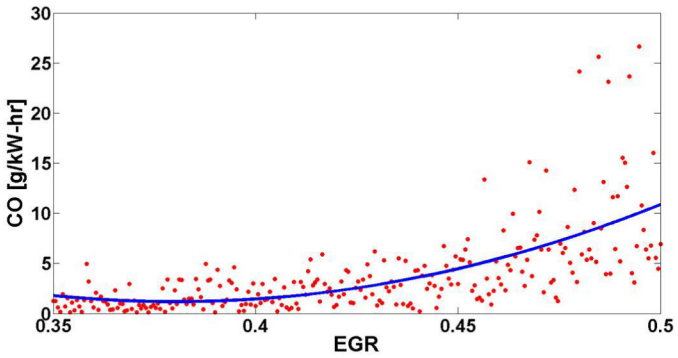

Figure 19. Scatter plot of CO emissions versus EGR. The blue curve is the corresponding regression fit.

Figure 18 also shows that UHC emissions are most sensitive to T_{IVC}. It is observed that UHC emissions decrease as T_{IVC} is raised (Figure 20). This trend is further investigated using brute force sensitivity analysis. Figure 21 shows the in-cylinder distributions of equivalence ratio and temperature at 30 °CA aTDC for two different cases. These cases have the exact same inputs as in the baseline case, except for different values of T_{IVC}, representing the extremes of the range over which T_{IVC} was varied for the GSA. It can be seen that for both cases, there are fuel-lean regions ($0.3 < \Phi < 0.6$) present near the cylinder head. However, these regions are smaller when T_{IVC} is higher (case (b)). In addition, the temperatures in these regions are higher for case (b). In fact, the minimum temperature in case (b) is around 100 K higher than case (a). These factors lead to a lower UHC production for case (b) (not shown here).

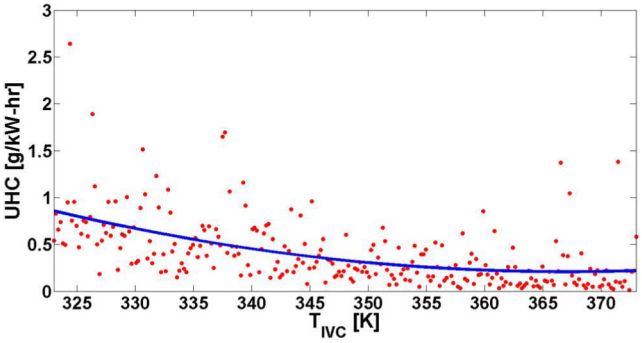

Figure 20. Scatter plot of UHC emissions versus T_{IVC}. The blue curve is the corresponding regression fit.

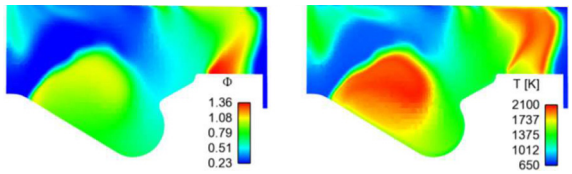

a.

Figure 21. In-cylinder equivalence ratio and temperature distributions along a cut-plane at 30 °CA aTDC for the [a] minimum (323 K) and [b] maximum (373 K) values of T_{IVC} noted in Table 2. All other input parameters are same as in the baseline case.

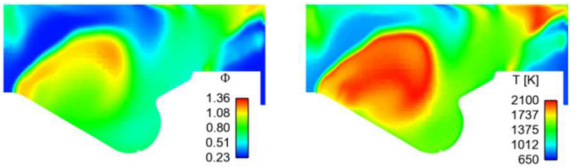

b.

Figure 21. (cont.) In-cylinder equivalence ratio and temperature distributions along a cut-plane at 30 °CA aTDC for the [a] minimum (323 K) and [b] maximum (373 K) values of T_{IVC} noted in Table 2. All other input parameters are same as in the baseline case.

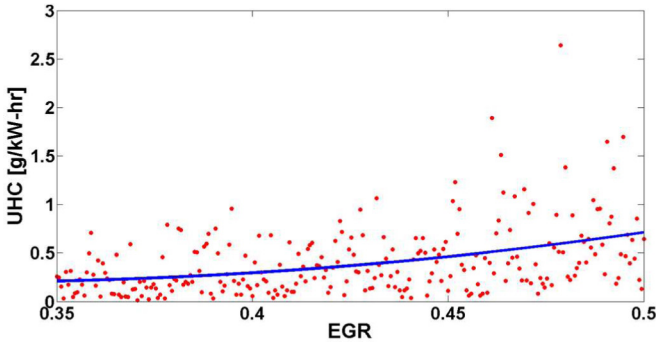

Figure 22. Scatter plot of UHC emissions versus EGR fraction. The blue curve is the corresponding regression fit.

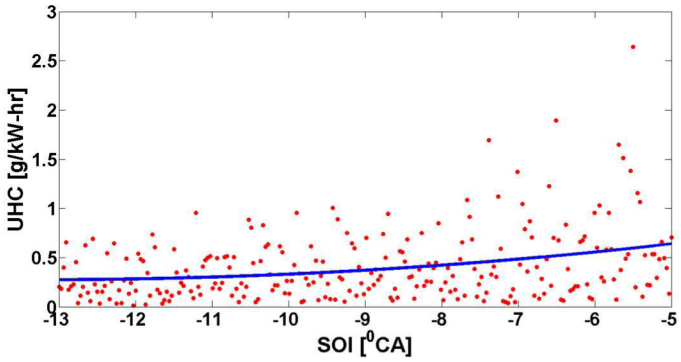

Figure 23. Scatter plot of UHC emissions versus SOI timing. The blue curve is the corresponding regression fit.

In addition to IVC temperature, EGR and SOI are also found to have a considerable influence on UHC emissions. Figures 22 and 23 depict the scatter plots of UHC emissions versus EGR and SOI respectively, along with corresponding regression fits. Clearly, UHC emissions are positively correlated to residual fraction and SOI timing.

Finally, the effect of the control variables on indicated specific fuel consumption (ISFC) is also assessed. The sensitivity coefficients are plotted in Figure 24. T_{IVC} and EGR seem to have the highest impact on ISFC, along with some minor influence of SOI timing and P_{IVC}. The scatter plots of ISFC versus T_{IVC} and EGR are shown in Figures 25 and 26, respectively. Clearly, ISFC is positively correlated to both these design parameters. This is mainly attributed to the fact that with higher T_{IVC} or higher EGR, the amount of oxygen in the cylinder gets lowered, with the effect of T_{IVC} being more pronounced. As a result, the indicated mean effective pressure (IMEP) decreases, thereby leading to an increase in ISFC.

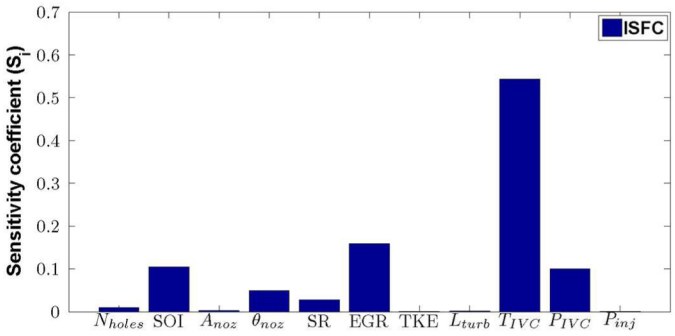

Figure 24. Sensitivity coefficients of different input variables for ISFC.

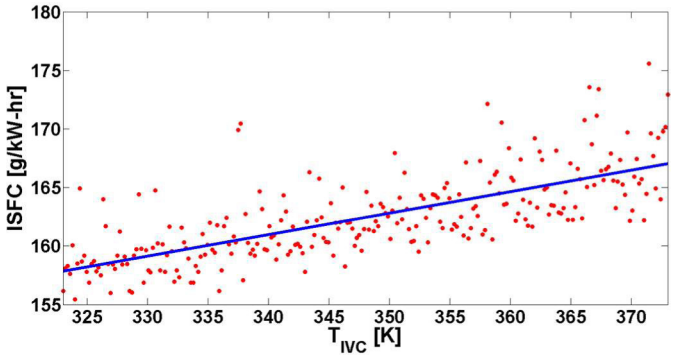

Figure 25. Scatter plot of ISFC versus T_{IVC}. The blue curve is the corresponding regression fit.

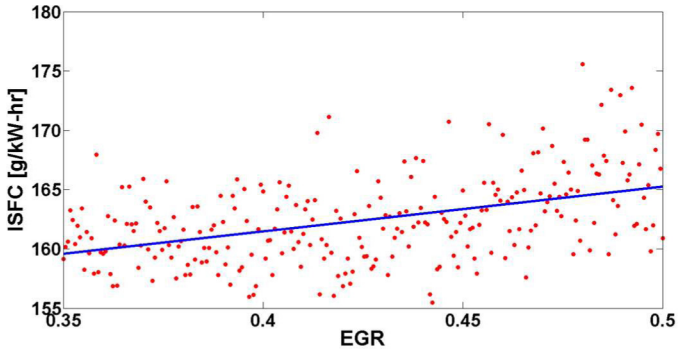

Figure 26. Scatter plot of ISFC versus EGR. The blue curve is the corresponding regression fit.

Peak Pressure and Maximum Pressure Rise Rate

The last set of targets comprises peak cylinder pressure and maximum pressure rise rate (MPRR), which define the mechanical limit of the engine. Figure 27 shows the sensitivities of both targets to the design variables. It can be seen that SOI timing has the highest impact on both of them. Earlier, it was found that retarding the SOI timing delayed both ignition timing and combustion phasing. This also leads to lower peak pressure and MPRR as shown in Figure 28. In addition, peak pressure is also influenced by P_{IVC}. As expected, higher IVC pressure leads to higher peak in-cylinder pressure (Figure 29). On the other hand, MPRR is found to be positively correlated to total nozzle area as reported in Figure 30. This is mainly due to better air utilization obtained with larger total nozzle area for gasoline-like fuels. Note that it is not the case for diesel as it requires smaller nozzle diameter for enhanced mixing [47]. Higher injection pressure, as shown in Figure 30, leads to higher maximum pressure rise rate.

This can be explained by the fact that an increase in injection pressure shortens the duration of fuel injection and increases injection velocity, thereby resulting in faster and better fuel-air mixing.

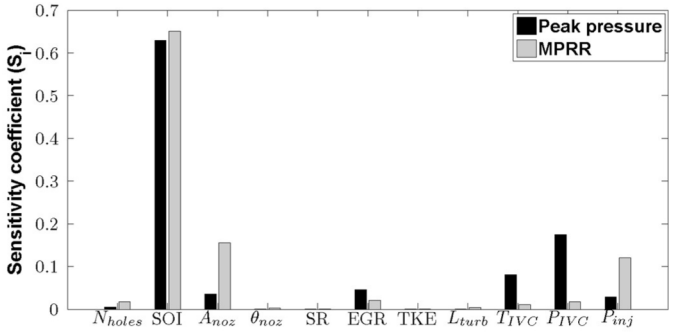

Figure 27. Sensitivity coefficients of different input variables for peak pressure and peak pressure rise rate.

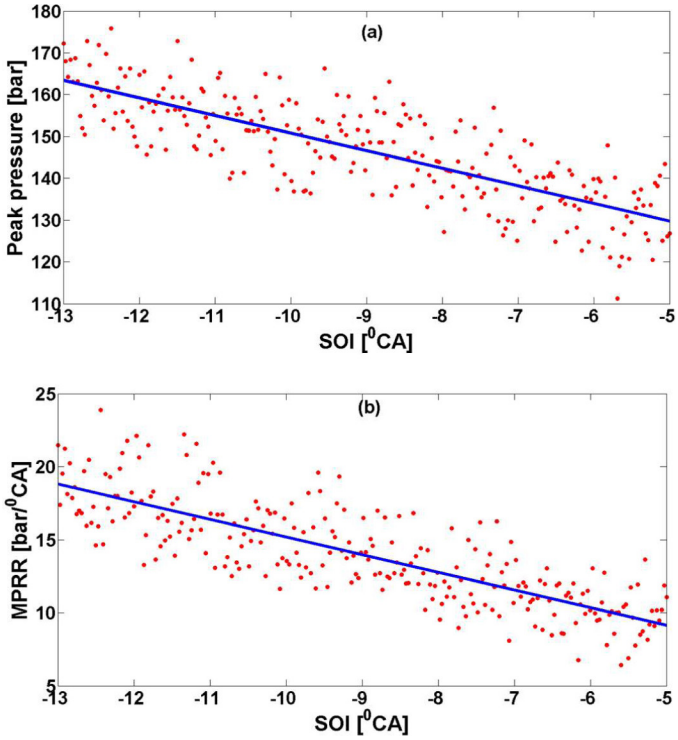

Figure 28. Scatter plots of [a] peak pressure and [b] maximum pressure rise rate versus SOI timing. The blue curves are the corresponding regression fits.

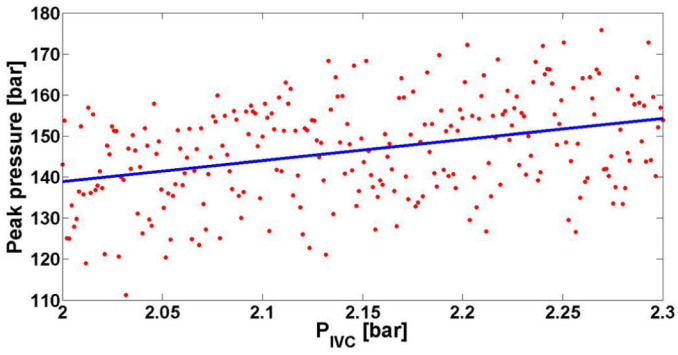

Figure 29. Scatter plot of peak pressure and versus P_{IVC}. The blue curve is the corresponding regression fit.

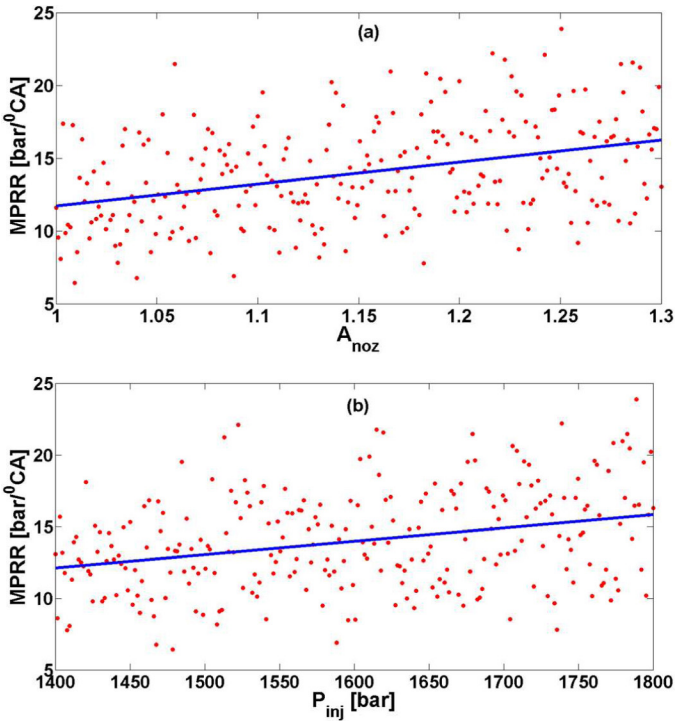

Figure 30. Scatter plots of maximum pressure rise rate versus [a] total nozzle area and [b] IVC pressure. The blue curves are the corresponding regression fits.

Finally, it is noted that the number of nozzle holes (N_{holes})do not affect any of the target variables investigated in the present study. This is not clear but could be possibly due to the fact that simulations were run only for a sector mesh with a single spray plume. This might not have been able to capture the effect of potentially different plume-to-plume interactions for different injector nozzle configurations. More studies using full engine cylinder geometry will be conducted in the future to investigate this aspect. Secondly, initial turbulence characteristics (TKE and L_{turb}) also play a negligible role. Indeed, brute force sensitivity analysis indicates that TKE is reduced to less than 1% of its initial value at IVC before SOI timing (not shown here). In addition, the GSA results also show that within the range of variation prescribed to all the input parameters, swirl ratio and nozzle inclusion angle have negligible impact on the target variables except CO emissions. Hence, the GSA methodology clearly shows parameters that may have a more profound influence on performance and emission characteristics of an engine.

SUMMARY AND CONCLUSIONS

In the present work, a GSA study was applied to heavy-duty CI engine combustion simulations with a gasoline-like fuel aimed at guiding engine design and optimization. A number of engine operating conditions, initial conditions and injector design parameters were chosen and their impact on multiple targets such as ignition timing, combustion phasing, overall burn duration, emissions and pressure rise rate was assessed. The GSA tool was used to screen key input parameters that affected various targets of interest most significantly and also provided guidance on the operating ranges of control variables to achieve combustion and performance robustness while pursuing higher efficiency. A total of 256 three-dimensional

CFD simulations were used in the GSA. The sensitivity of the targets to each input variable was quantified in terms of sensitivity coefficients. The main findings of the study are as follows.

- It was found that ignition timing (CA2, CA10) was affected by SOI timing the most and a positive correlation was observed between them, similar to conventional diesel combustion. Unlike CA2 which was solely dominated by SOI, CA10 displayed a certain degree of controllability through EGR, T_{IVC} or P_{IVC} besides SOI.
- For combustion phasing (CA50, CA90), although SOI was again found to be the most sensitive variable, EGR fraction and IVC temperature also played an important role, especially for CA90. Moreover, SOI and EGR were found to be equally effective in influencing CA90.
- EGR was the most effective way of controlling burn duration. However, T_{IVC}, P_{IVC} and injection pressure could also be considered to achieve the optimal fuel efficiency.
- NOx was primarily affected by EGR similar to conventional mixing-controlled combustion. SOI might play a certain role more towards relatively lower EGR level. EGR and T_{IVC} were the major players in controlling soot and it might be able to find a window of low soot levels at relatively lower EGR and T_{IVC}.
- Unlike NOx and soot, T_{IVC} was the dominant factor for HC emissions. To maintain a lower level of HC emissions, low T_{IVC} should be avoided.
- T_{IVC} and EGR were the most important input variables affecting ISFC as a result of their direct impact on the amount of oxygen present in the in-cylinder mixture.
- In addition, peak in-cylinder pressure and MPRR were most significantly affected by the SOI timing. However, MPRR was also influenced by total nozzle area and injection pressure by way of modulating fuel-air mixing in the cylinder. The corresponding scatter plots provided additional insights that could be useful in determining a smaller design parameter space spanned by narrower ranges of only the important control variables, for a more rigorous design optimization.

In the future work, a more detailed investigation of the important inputs identified in this GSA will be carried out and coupled with engine piston bowl design to optimize engine efficiency and emissions. In addition, it is noted that the present work didn't investigate the impact of uncertainties in CFD model parameters and chemical kinetics. These aspects will also be explored in future studies.

REFERENCES

1. U.S. Energy Information administration at: http://www.eia.gov/tools/faqs/faq.cfm?id=447&t=1.
2. U.S. Energy Information administration at http://www.eia.gov/forecasts.
3. Reitz, R., "Combustion and Ignition Chemistry in Internal Combustion Engines", *Int. J. Engine Res.* 14(5): 411–415, 2013, doi:10.1177/1468087413498047.
4. World Energy Council. Global Transport Scenarios 2050. WEC London, 2011.
5. Reitz, R., "Directions in Internal Combustion Engine Research", *Combust. Flame.* 160: 1–8, 2013, doi:10.1016/j.combustflame.2012.11.002.
6. Kalghatgi, G., "The Outlook for Fuels for Internal Combustion Engines", *Int. J. Engine Res.* 15(4): 383–398, 2014, doi:10.1177/1468087414526189.
7. Kalghatgi, G., "Developments in Internal Combustion Engines and Implications for Combustion Science and Future Transport Fuels", *Proc. Combust. Inst.* 35(1): 101–115, 2015, doi:10.1016/j.proci.2014.10.002.
8. Dec, J., "Advanced Compression-ignition Engines -Understanding the In-cylinder Processes", *Proc. Combust. Inst.* 32:2727–2742, 2009, doi:10.1016/j.proci.2008.08.008.
9. Kalghatgi, G., "Fuel/Engine Interactions," (Warrendale, SAE International, 2013), doi:10.4271/R-409.
10. Kalghatgi, G., Hildingsson, L., Harrison, A., and Johansson, B., "Surrogate Fuels for Premixed Combustion in Compression Ignition Engines", *Int. J. Engine Res.* 12(5): 452–465, 2011, doi:10.1177/1468087411409307.
11. Kalghatgi, G., Risberg, P., and Angstrom, H., "Advantages of Fuels with High Resistance to Auto-ignition in Late-injection, Low-temperature, Compression Ignition Combustion," SAE Technical Paper 2006-01-3385, 2006, doi:10.4271/2006-01-3385.
12. Kalghatgi, G., Risberg, P., and Ångström, H., "Partially Pre-Mixed Auto-Ignition of Gasoline to Attain Low Smoke and Low NOx at High Load in a Compression Ignition Engine and Comparison with a Diesel Fuel," SAE Technical Paper 2007-01-0006, 2007, doi:10.4271/2007-01-0006.
13. Hildingsson, L., Johansson, B., Kalghatgi, G., and Harrison, A., "Some Effects of Fuel Autoignition Quality and Volatility in Premixed Compression Ignition Engines," *SAE Int. J. Engines* 3(1):440–460, 2010, doi:10.4271/2010-01-0607.
14. Sellnau, M., Foster, M., Hoyer, K., Moore, W., "Development of a Gasoline Direct Injection Compression Ignition (GDCI) Engine," *SAE Int. J. Engines* 7(2):835–851, 2014, doi:10.4271/2014-01-1300.
15. Chang, J., Viollet, Y., Amer, A., and Kalghatgi, G., "Fuel Economy Potential of Partially Premixed Compression Ignition (PPCI) Combustion with Naphtha Fuel," SAE Technical Paper 2013-01-2701, 2013, doi:10.4271/2013-01-2701.
16. Zhou, D.Y., Davis, M.J. and Skodje, R.T., "Multitarget Global Sensitivity Analysis of n-Butanol Combustion", *J. Phys. Chem. A*, 117(17): 3569–3584,2013, doi:10.1021/jp312340q.
17. Scire, J. J., Jr.Dryer F. L., and Yetter, R.A., "Comparison of Global and Local Sensitivity Techniques for Rate Constants Determined Using Complex Reaction Mechanisms", *Int. J. Chem. Kinet.* 33: 784–802, 2011, doi:10.1002/kin.10001.
18. Zador, J., Zseley I. G., and Turanyi, T., "Local and Global Uncertainty Analysis of Complex Chemical Kinetic Systems", *Reliab. Eng. Syst. Saf.* 91: 1232–1240, 2006, doi:10.1016/j.ress.2011.11.020.
19. Wang, H., Reitz, R., and Yao, M., "Comparison of Diesel Combustion CFD Models and Evaluation of the Effects of Model Constants," SAE Technical Paper 2012-01-0134, 2012, doi:10.4271/2012-01-0134.
20. Saltelli, A., Ratto, M., Andres, T., Campolongo, F., "Global sensitivity Analysis: The Primer",Wiley, 2008.
21. Pei, Y., Shan, R., Som, S., Lu, T., "Global Sensitivity Analysis of a Diesel Engine Simulation with Multi-Target Functions," SAE Technical Paper 2014-01-1117, 2014, doi:10.4271/2014-01-1117.
22. Pei, Y., Davis, M. J., Pickett, L. M., and Som, S., "Engine Combustion Network (ECN): Global sensitivity analysis of Spray A for different combustion vessels", *Combust. Flame*, 162(6): 2337–2347, 2015, doi:10.1016/j.combustflame.2015.11.024.
23. http://www.sandia.gov/ecn/workshop/ECN3.php.
24. Kodavasal, J., Pei, Y., Harms, K., Ciatti, S., "Global Sensitivity Analysis of a Gasoline Compression Ignition Engine Simulation with Multiple Targets on an IBM Blue Gene/Q Supercomputer," SAE Technical Paper 2016-01-0602, 2016, doi:10.4271/2016-01-0602.
25. Kodavasal, J., Dam, N.V., Pei, Y., Harms, K., "Sensitivity analysis on key CFD model inputs for gasoline compression ignition on IBM Blue Gene/Q supercomputer," *THIESEL 2016 Conference on Thermo- and Fluid Dynamic Processes in Direct Injection Engines*, September 2016.
26. CONVERGE 2.3 Theory Manual, Convergent Science, Inc., Middleton, WI, 2016.
27. Han, Z. and Reitz, R. D., "Turbulence Modeling of Internal Combustion Engines Using RNG k-ε Models," *Combust. Sci. and Tech.*, 106: 267–295, 1995, doi:10.1080/00102209508907782.
28. Reitz, R. and Diwakar, R., "Structure of High-Pressure Fuel Sprays," SAE Technical Paper 870598, 1987, doi:10.4271/870598.
29. Reitz, R.D., "Modeling Atomization Processes in High Pressure Vaporizing Sprays," *Atomization and Spray Tech.* 3: 309–337, 1987.

30. Patterson, M. and Reitz, R., "Modeling the Effects of Fuel Spray Characteristics on Diesel Engine Combustion and Emission," SAE Technical Paper 980131, 1998, doi:10.4271/980131.
31. Schmidt, D.P. and Rutland, C.J., "A New Droplet Collision Algorithm," *J. Comp. Phys.* 164: 62–80, 2000, doi:10.1006/jcph.2000.6568.
32. Frossling, N. "Evaporation, heat transfer, and velocity distribution in two-dimensional and rotationally symmetrical laminar boundary-layer flow," *N.A.C.A.* 168: AD-B189, 1956.
33. Liu, A., Mather, D., and Reitz, R., "Modeling the Effects of Drop Drag and Breakup on Fuel Sprays," SAE Technical Paper 930072, 1993, doi:10.4271/930072.
34. Amsden, A.A., O'Rourke, P.J. and Butler, T.D., "KIVA-II: A Computer Program for Chemically Reactive Flows with Sprays", Los Alamos National Laboratory Report No. LA-11560-MS, 1989.
35. Liu, Y-D., Jia, M., Xie, M-Z., and Pang, B., "Enhancement on a skeletal kinetic model for Primary Reference Fuel oxidation by using a semi-decoupling methodology," *Energy and Fuels*, 26 (12): 7069–7083, 2012, doi:10.1021/ef301242b.
36. Bae, C. and Kim, J., "Alternative Fuels for Internal Combustion Engines", *Proc. Combust. Inst.* 2016, doi:10.1016/j.proci.2016.09.009.
37. Heywood J.B., "Internal Combustion Engine Fundamentals," McGraw-Hill Inc, 1998.
38. Hiroyasu, H. and Kadota, T., "Models for Combustion and Formation of Nitric Oxide and Soot in Direct Injection Diesel Engines," SAE Technical Paper 760129, 1976, doi:10.4271/760129.
39. Nagle, J. and Strickland-Constable, R. F., "Oxidation of Carbon Between 1000-2000 C," *Proc. of the Fifth Carbon Conf.*, Vol. 1, p. 154, 1962.
40. Senecal, P., Pomraning, E., Richards, K., Briggs, T., "Multi-Dimensional Modeling of Direct-Injection Diesel Spray Liquid Length and Flame Lift-off Length using CFD and Parallel Detailed Chemistry," SAE Technical Paper 2003-01-1043, 2003, doi:10.4271/2003-01-1043.
41. Babajimopoulos A., Assanis D.N., Flowers D.L., Aceves S.M., Hessel R.P., "A fully coupled computational fluid dynamics and multi-zone model with detailed chemical kinetics for the simulation of premixed charge compression ignition engines," *Int. J. Engine Res.* 6(5): 497–512, 2005, doi:10.1243/146808705X30503.
42. Pal, P., Keum, S. and Im, H.G., "Assessment of flamelet versus multi-zone combustion modeling approaches for stratified-charge compression ignition engines", *Int. J. Engine Res.* 17(3): 280–290, 2016, doi:10.1177/1468087415571006.
43. Pal, P., "Computational modeling and analysis of low temperature combustion regimes for advanced engine applications", *Ph.D. Dissertation*, University of Michigan-Ann Arbor, 2016, http://hdl.handle.net/2027.42/120735.
44. Keum, S., Pal, P., Im, H.G., Babajimopoulos, A., "Effects of fuel injection parameters on the performance of homogeneous charge compression ignition at low-load conditions", *Int. J. Engine Res.* 17(4): 413–420, 2016, doi:10.1177/1468087415583597.
45. Pickett, L., Bruneaux, G., and Payri, R., *Engine Combustion Netwrok*, 2014, http://public.ca.sandia.gov/ecn/.
46. Contino, F., Masurier, J.-B., Foucher, F., Lucchini, T., "CFD Simulations Using the TDAC Method to Model Isooctane Combustion for a Large Range of Ozone Seeding and Temperature Conditions in a Single Cylinder HCCI Engine", *Fuel.* 137: 179–184, 2014, doi:10.1016/j.fuel.2014.07.084.
47. Pei, Y., Zhang, Y., Kumar, P., Traver, M., "CFD-Guided Heavy Duty Mixing Controlled Combustion System Optimization with a Gasoline-Like Fuel," SAE Technical Paper 2017-01-0550, 2017, doi:10.4271/2017-01-0550.

CONTACT INFORMATION

Pinaki Pal, Ph.D.
Post-doctoral appointee
Argonne National Laboratory
9700 S. Cass Avenue
Lemont, IL- 60439
pal@anl.gov

ACKNOWLEDGMENTS

The submitted manuscript has been created by UChicago Argonne, LLC, Operator of Argonne National Laboratory (Argonne). Argonne, a U.S. Department of Energy Office (DOE) of Science laboratory, is operated under Contract No. DE-AC02- 06CH11357. The U.S. Government retains for itself, and others acting on its behalf, a paid-up nonexclusive, irrevocable worldwide license in said article to reproduce, prepare derivative works, distribute copies to the public, and perform publicly and display publicly, by or on behalf of the Government.

This research used resources of the Argonne Leadership Computing Facility (ALCF), which is a DOE Office of Science User Facility supported under contract DE-AC02-06CH11357. Fusion and Blues High Performance LCRC cluster facilities at Argonne National Laboratory were also used for some of the simulations.

The authors would like to thank Aramco Services Company: Aramco Research Center - Detroit, for funding the project that led to this work; We also thank Dr. Noah Van Dam and Dr. Muhsin Ameen from Argonne National Laboratory for many helpful discussions and Convergent Science Inc. for providing the Converge CFD software licenses.